Pulsed High-Frequency EPR Study on the Location of Carotenoid and Chlorophyll Cation Radicals in Photosystem II

K. V. Lakshmi,[†] Oleg G. Poluektov,[‡] Michael J. Reifler,[†,§] Arlene M. Wagner,[‡]
Marion C. Thurnauer,*[‡] and Gary W. Brudvig*[,†]

*Contribution from the Department of Chemistry, Yale University, P.O. Box 208107,
New Haven, Connecticut 06520-8107, and Chemistry Department, Argonne National Laboratory,
9700 S. Cass Ave., Argonne, Illinois 60439*

Received December 3, 2002; E-mail: gary.brudvig@yale.edu; mariont@anl.gov

Abstract: When the primary electron-donation pathway from the water-oxidation complex in photosystem II (PS II) is inhibited, chlorophyll (Chl_Z and Chl_D), β-carotene (Car) and cytochrome b_{559} are alternate electron donors that are believed to function in a photoprotection mechanism. Previous studies have demonstrated that high-frequency EPR spectroscopy (at 130 GHz), together with deuteration of PS II, yields resolved Car^+ and Chl^+ EPR signals (Lakshmi et al. *J. Phys. Chem. B* **2000**, *104*, 10 445−10 448). The present study describes the use of pulsed high-frequency EPR spectroscopy to measure the location of the carotenoid and chlorophyll radicals relative to other paramagnetic cofactors in *Synechococcus lividus* PS II. The spin−lattice relaxation rates of the Car^+ and Chl^+ radicals are measured in manganese-depleted and manganese-depleted, cyanide-treated PS II; in these samples, the non-heme Fe(II) is high-spin ($S = 2$) and low-spin ($S = 0$), respectively. The Car^+ and Chl^+ radicals exhibit dipolar-enhanced relaxation rates in the presence of high-spin ($S = 2$) Fe(II) that are eliminated when the Fe(II) is low-spin ($S = 0$). The relaxation enhancements of the Car^+ and Chl^+ by the non-heme Fe(II) are smaller than the relaxation enhancement of $Tyr_D^{\bullet}$ and P_{865}^+ by the non-heme Fe(II) in PS II and in the reaction center from *Rhodobacter sphaeroides*, respectively, indicating that the Car^+−Fe(II) and Chl^+-Fe(II) distances are greater than the known $Tyr_D^{\bullet}$−Fe(II) and P_{865}^+−Fe(II) distances. The Car^+ radical exhibits a greater relaxation enhancement by Fe(II) than the Chl^+ radical, consistent with Car being an earlier electron donor to P_{680}^+ than Chl. On the basis of the distance estimates obtained in the present study and by analogy to carotenoid-binding sites in other pigment−protein complexes, possible binding sites are discussed for the Car cofactors in PS II. The relative location of Car^+ and Chl^+ radicals determined in this study provides valuable insight into the sequence of electron transfers in the alternate electron-donation pathways of PS II.

Introduction

Photoexcitation of the primary-donor chlorophyll, P_{680}, of photosystem II (PS II) results in a series of rapid electron-transfer steps in the primary electron-transfer pathway that result in the breakdown of water to dioxygen and the generation of reducing equivalents for use in the chain of photosynthetic reactions (for review see Debus, 1992).[1] It has recently been shown that in plants and cyanobacteria there are secondary electron-transfer pathways that are of importance in quenching reactive forms of photoinduced radicals in PS II. In the event that electron transfer from the water-oxidation complex to P_{680}^+ is blocked, these alternate secondary electron-transfer pathways are active. P_{680}^+ radicals formed upon photoexcitation are rapidly quenched by electrons from cytochrome b_{559} (cyt b_{559}), monomeric chlorophyll (Chl) and β-carotene (Car) cofactors in the PS II complex. It is proposed that these secondary electron-transfer pathways are important for photoprotection of

PS II (for a review, see Stewart and Brudvig, 1998).[2] To date, however, the sequence of electron-transfer events in the secondary electron-transfer pathways of PS II and the locations of the redox-active Chl and Car cofactors remain uncertain.

The Car^+ and Chl^+ radicals of PS II have been studied by optical, Raman, FTIR, X-band and high-frequency (130 and 285 GHz) EPR spectroscopy.[3−11] In these studies, the Car^+ and Chl^+ radicals were generated by low-temperature illumination of PS

† Yale University.

‡ Argonne National Laboratory.

§ Present address: 454 Corporation, 20 Commercial Street, Branford, CT 06405.

(1) Debus, R. J. *Biochim. Biophys. Acta* **1992**, *1102*, 269−352.

(2) Stewart, D. H.; Brudvig, G. W. *Biochim. Biophys. Acta* **1998**, *1367*, 63−87.

(3) (a) Schenck, C.; Diner, B. A.; Mathis, P.; Satoh, K. *Biochim. Biophys. Acta* **1982**, *680*, 216−227. (b) Noguchi, T.; Mitsuka, T.; Inoue, V. *FEBS Lett.* **1994**, *356*, 179−182. (c) Hillmann, B.; Schlodder, E. *Biochim. Biophys. Acta* **1995**, *1231*, 76−88.

(4) Lakshmi, K. V.; Reifler, M. J.; Brudvig, G. W.; Poluektov, O. G.; Wagner, A. M.; Thurnauer, M. C. *J. Phys. Chem. B* **2000**, *104*, 10 445−10 448.

(5) Faller, P.; Rutherford, A. W.; Un, S. *J. Phys. Chem. B* **2000**, *104*, 10 960−10 963.

(6) Faller, P.; Pascal, A.; Rutherford, A. W. *Biochemistry* **2001**, *40*, 6431−6440.

(7) Faller, P.; Maly, T.; Rutherford, A. W.; MacMillan, F. *Biochemistry* **2001**, *40*, 320−326.

(8) Hanley, J.; Deligiannakis, Y.; Pascal, A.; Faller, P.; Rutherford, A. W. *Biochemistry* **1999**, *38*, 8189−8195.

(9) Tracewell, C. A.; Cua, A.; Stewart, D. H.; Bocian, D. F.; Brudvig, G. W. *Biochemistry* **2001**, *40*, 193−203.

(10) Vrettos, J. S.; Stewart, D. H.; de Paula, J. C.; Brudvig, G. W. *J. Phys. Chem. B* **1999**, *103*, 6403−6406.

Scheme 1. Pathways for Secondary Photoprotective Electron Transfer in PS II

(a)
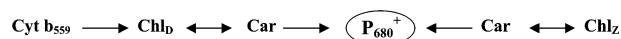
(b)
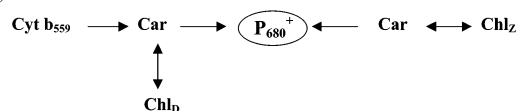

(c)

D2 polypeptide   *D1 polypeptide*

Three possible pathways involving Cyt b_{559}, Car, and Chl are proposed on the D2-side of PS II: (a) A linear pathway (where the electron is transferred from Cyt b_{559} to Chl to Car), (b) parallel pathways (where there are independent pathways of electron donation from Cyt b_{559} to Chl and Car), and (c) a branched pathway (where Cyt b_{559} and Chl donate electrons to the Car which is responsible for the rereduction of P_{680}^+). In each case, another electron-transfer pathway could exist on the D1 polypeptide that involves either the Car or Chl donors.

II samples from cyanobacteria and spinach. On the basis of these studies, several possible pathways for secondary electron transfer have been proposed in PS II (Scheme 1). In addition to studies aimed at understanding the sequence and kinetics of secondary electron transfer in PS II, several studies have also been conducted to determine the stoichiometry and structural characteristics of the cofactors involved in the secondary electron pathways of PS II.[4,5,7,10−16] Cofactor extraction procedures on PS II have indicated that there exist two monomeric chlorophyll (Chl$_D$ and Chl$_Z$) and two β-carotene cofactors in the PS II RC.[17−19] In contrast, X-ray crystallography studies have shown that the bacterial reaction center, which shares a high degree of homology with PS II, contains only a single copy of a sphaeroidene in the cis conformation. The orientation of the transition dipole moment of the Car molecules within the PS II membrane plane has been studied by linear dichroism.[12,13] This work has suggested that the orientations of the two Car molecules in the D1 and D2 polypeptide are different from each other. Circular dichroism has suggested that the two Car molecules are excitonically coupled and may be placed in close proximity of each other in the PS II reaction center.[14] On the

basis of these and other results, it has recently been proposed that both Car molecules in PS II are redox active; however, only one Car is involved in cyclic electron transfer via Cyt b_{559}.[15] High-frequency EPR and ENDOR studies have shown that the electronic structures of the Car$^+$ and Chl$^+$ radicals in PS II[4,5] are similar to those of model canthaxanthin radicals on solid alumina support and Chl a in solution,[20] respectively. High-frequency EPR, ENDOR, and resonance Raman spectroscopy of Car$^+$ and Chl$^+$ radicals also indicate that the charge is delocalized along the length of the carotenoid chain and over the tetrapyrrole ring of the Car$^+$ and Chl$^+$ radicals, respectively.[7,21,22]

The 3.8 Å resolution X-ray crystallography structure[23] and cryo-electron microscopy structures of PS II[24−29] reveal the position of the tetranuclear manganese cluster, non-heme Fe(II), primary-donor chlorophyll (P$_{680}$), accessory chlorophylls, pheophytin, primary quinone and cyt b_{559} cofactors. It is observed that the cofactors are arranged with a pseudo-C_2 symmetry about the non-heme Fe(II) center of PS II. At the current resolution of PS II structures, the locations of the β-carotene cofactors are unknown. Previous mutagenesis studies have indicated that the redox-active monomeric Chl participating in the secondary electron-transfer pathway of *Synechocystis* PCC 6803 PS II is ligated to His-118 on the D1 polypeptide.[30,31] The location of the monomeric chlorophylls ligated to His-118 and His-117 residues in the D1 and D2 polypeptides, respectively, are confirmed by the X-ray crystallography structure.[23] However, the X-ray crystallography structure of PS II places Cyt b_{559} proximal to the D2 polypeptide which raises questions on the sequence of cyclic electron transfer via Cyt b_{559} in the secondary electron-transfer pathway of PS II. It has been suggested that both monomeric Chls may participate in electron-transfer events, either in separate electron-transfer pathways or by rapid hole-equilibration across the cofactor radicals in PS II (Scheme 1).[9] It is essential to determine the location of the redox-active Car and Chl cofactors in PS II to clarify the electron-transfer events in the secondary electron-transfer pathway of PS II. Structural studies of the PS II complex (molecular weight $\approx$ 600 kDa) have been challenging due to the difficulty in preparing high diffraction-quality crystals and the presence of paramagnetic electron-transfer cofactors.

Electron spin−lattice relaxation rate constants can be used to determine the location, orientation and magnetic properties of paramagnetic centers in native membrane-bound PS II

(11) Pascal, A.; Telfer, A.; Barber, J.; Robert, B. *FEBS Lett.* **1999**, *453*, 11−14.
(12) van Dorssen, R. J.; Breton, J.; Plijter, J. J.; Satoh, K.; van Gorkom, H. J.; Amesz, J. *Biochim. Biophys. Acta* **1987**, *893*, 267−274.
(13) Newell, W. R.; van Amerongen, H.; Barber, J.; van Grondelle, R. *Biochim. Biophys. Acta* **1991**, *1057*, 232−238.
(14) Tetenkin, V. L.; Gulyaev, B. A.; Seibert, M.; Rubin, A. B. *FEBS Lett.* **1989**, *250*, 459−463.
(15) Telfer, A. *Philos. Trans. R. Soc. London B* **2002**, *357*, 1431−1440.
(16) Deligiannakis, Y.; Hanley, J.; Rutherford, A. W. *J. Am. Chem. Soc.* **2000**, *122*, 400−401.
(17) De Las Rivas, J.; Telfer, A.; Barber, J. *Biochim. Biophys. Acta* **1993**, *1142*, 155−164.
(18) Kurreck, J.; Liu, B. N.; Napiwotzki, A.; Sellin, S.; Eckert, H. J.; Eichler, H. J.; Renger, G. *Biochim. Biophys. Acta* **1997**, *1318*, 307−315.
(19) Tomo, T.; Mimuro, M.; Iwaki, M.; Kobayashi, M.; Itoh, S.; Satoh, K. *Biochim. Biophys. Acta* **1997**, *1321*, 21−20.

(20) Konovalova, T. A.; Krzystek, J.; Bratt, P. J.; van Tol, J.; Brunel, L. C.; Kispert, L. D. *J. Phys. Chem. B* **1999**, *103*, 5782−5786.
(21) Jeevarajan, A. S.; Kispert, L. D.; Piekara-Sady, L. *Chem. Phys. Lett.* **1993**, *209*, 269−274.
(22) Jeevarajan, A. S.; Kispert, L. D.; Chumanov, G.; Zhou, C.; Cotton, T. M. *Chem. Phys. Lett.* **1996**, *259*, 515−522.
(23) Zouni, A.; Witt, H. T.; Kern, J.; Fromme, P.; Krauss, N.; Saenger, W.; Orth, P. *Nature* **2001**, *409*, 739−743.
(24) Hankamer, B.; Morris, E.; Nield, J.; Gerle, C.; Barber, J. *J. Struct. Biol.* **2001**, *135*, 262−269.
(25) Nield, J.; Kruse, O.; Ruprecht, J.; da Fonseca, P.; Buchel, C.; Barber, J. *J. Biol. Chem.* **2000**, *275*, 27 940−27 946.
(26) Nield, J.; Orlova, E. V.; Morris, E. P.; Gowen, B.; van Heel, M.; Barber, J. *Nature Struct. Biol.* **2000**, *7*, 44−47.
(27) Hankamer, B.; Morris, E. P.; Barber, J. *Nature Struct. Biol.* **1999**, *6*, 560−564.
(28) Rhee, K. H.; Morris, E. P.; Barber, J.; Kühlbrandt, W. *Nature* **1998**, *396*, 283−286.
(29) Rhee, K. H.; Morris, E. P.; Zheleva, D.; Hankamer, B.; Kühlbrandt, W.; Barber, J. *Nature* **1997**, *389*, 522−526.
(30) Stewart, D. H.; Cua, A.; Chisholm, D. A.; Diner, B. A.; Bocian, D. F.; Brudvig, G. W. *Biochemistry* **1998**, *37*, 10 040−10 046.
(31) Schelvis, J. P. M.; Vannoort, P. I.; Aartsma, T. J.; van Gorkom, H. J. *Biochim. Biophys. Acta* **1994**, *1184*, 242−250.

complexes. The proximity of radical species to a paramagnetic metal center ($r < 40$ Å) enhances the spin−lattice relaxation of the radical by an orientation-dependent dipole−dipole interaction.[32] The spin−lattice relaxation rate constants resulting from the dipole−dipole interaction can be used to probe the distance between the interacting centers in PS II.[33,34] For example, in the absence of the X-ray crystallography and electron-microscopy structures of PS II, saturation-recovery EPR spectroscopy at X-band frequency was successfully employed to establish early evidence of the symmetric location of the redox-active tyrosine residues (Tyr$_D$ and Tyr$_Z$) of PS II.[35]

In principle, a similar X-band saturation-recovery EPR approach can be used to determine the relative location of the Car$^+$ and Chl$^+$ radicals of PS II. However, Car$^+$ and Chl$^+$ radicals yield unresolved EPR signals at X-band frequency.[8,36] The EPR signals of organic radicals in proteins have previously been partially resolved either by the use of microwave frequency as high as 285 GHz[5] or by the observation of radicals with relatively large **g**-anisotropy at 139.5 GHz.[37] Deuteration of PS II samples to reduce the inhomogeneous broadening of EPR resonances has permitted the observation of resolved EPR signals of the Car$^+$ and Chl$^+$ radicals of PS II at D-band (130 GHz) EPR frequency.[4] In this study, we demonstrate the combined use of deuteration of *Synechococcus lividus* PS II and pulsed high-frequency (130 GHz) saturation-recovery EPR spectroscopy to measure directly the spin−spin interaction of the Car$^+$ and Chl$^+$ radicals with other paramagnetic centers of PS II. This is the first use of high-frequency D-band (130 GHz) saturation-recovery EPR spectroscopy of deuterated PS II complexes to directly probe the locations of redox centers in an electron-transfer protein complex.

We find that the Car$^+$ radicals exhibit dipolar-enhanced spin−lattice relaxation when the Fe(II) in PS II is high-spin ($S = 2$) that is eliminated when the Fe(II) is low-spin ($S = 0$). The spin−lattice relaxation enhancement of Car$^+$ by high-spin Fe(II) is smaller than the relaxation enhancement of Tyr$_D$• by high-spin Fe(II), indicating that the Car$^+$−Fe(II) distance is greater than the known Tyr$_D$•−Fe(II) distance in PS II. The Car$^+$ exhibits greater relaxation enhancement by high-spin Fe(II) than Chl$^+$ indicating that the Car$^+$ radical is closer to the non-heme Fe-(II) than the Chl$^+$ radical in the secondary electron-transfer pathway of PS II. This is consistent with the Car being an earlier electron donor to P$_{680}^+$ than the Chl. On the basis of the Car$^+$−Fe(II) and Chl$^+$−Fe(II) distance estimates obtained in this study and by analogy to the location and nature of the carotenoid-binding sites in the reaction center from *Rps. viridis*[38] and the LH−II complex from *Rhodospirillum molischianum*,[39] we propose possible β-carotene binding sites in PS II.
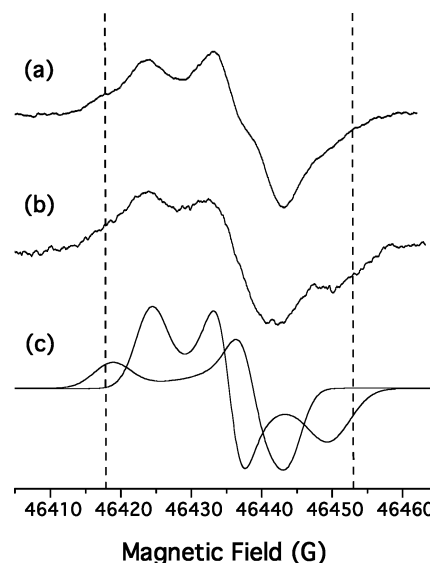

Figure 1. Experimental high-frequency (130 GHz) *cw* EPR difference spectrum of Car$^+$ and Chl$^+$ radicals in PS II illuminated at (a) 85 K and (b) 190 K. (c) Simulated spectra of Car$^+$ and Chl$^+$ radicals in PS II using g-tensors for the individual species as reported previously.[4] The dashed lines highlight the magnetic-field positions used for saturation-recovery measurements of Car$^+$ and Chl$^+$ radicals, respectively.

Materials and Methods

Sample Preparation. It has previously been demonstrated that deuteration of PS II samples yields resolved EPR signals of the Car$^+$ and Chl$^+$ radicals at D-band (130 GHz) EPR frequency.[4] For the present study, deuterated *Synechococcus lividus* cells were grown at 30 °C in Ac medium containing D$_2$O[40,41] and deuterated PS II core complexes were isolated by previously described procedures.[4] Manganese depletion of deuterated PS II core complexes was carried out with hydroxylamine[42] and cyanide treatment of deuterated manganese-depleted PS II core complexes was done as described by Sanakis et al.[43] Reaction centers from the photosynthetic bacterium *Rb. sphaeroides* R-26 were isolated as previously described by Utschig et al.[44] Bacterial RC concentrations were determined with the extinction coefficient $\epsilon_{802} = 288$ mM^{-1} cm^{-1}.[45]

Trapping of Redox-Active Cofactors in Paramagnetic States. Deuterated PS II samples for high-frequency D-band EPR measurements ([Chl] $\approx$ 8 mg/mL in buffer containing 20 mM CaCl$_2$, 5 mM MgCl$_2$, 50 mM MES, pH 6.0 with 20% (w/v) glycerol and 0.03% (w/v) β-dodecyl maltoside) were preincubated in the dark at 0 °C with 200 μM potassium ferricyanide prior to loading into 0.4 mm I. D. quartz capillary tubes. Tyr$_D$• radicals were generated by a 10 min illumination at 0 °C and 3 min dark incubation at 0 °C prior to freezing to 60 K in the EPR cavity. Car$^+$ and Chl$^+$ radicals were generated by illumination at 85 or 190 K inside the EPR cavity as previously described (Figure 1).[4] High-frequency saturation-recovery EPR measure-

(32) Hirsh, D. J.; Beck, W. F.; Innes, J. B.; Brudvig, G. W. *Biochemistry* **1992**, *31*, 532−541.
(33) Lakshmi, K. V.; Brudvig, G. W. In *Distance Measurements in Biological Systems by EPR*; Berliner, L. J., Eaton, S. S., Eaton, G. R., Ed.; Kluwer Academic/ Plenum Publishers: New York, 2000; Vol. 19 of Biological Magnetic Resonance, pp 513−567.
(34) Lakshmi, K. V.; Brudvig, G. W. *Curr. Opin. Struct. Biol.* **2001**, *11*, 523−531.
(35) Koulougliotis, D.; Tang, X.-S.; Diner, B. A.; Brudvig, G. W. *Biochemistry* **1995**, *34*, 2850−2856.
(36) Koulougliotis, D.; Innes, J. B.; Brudvig, G. W. *Biochemistry* **1994**, *33*, 11 814−11 822.
(37) Farrar, C. T.; Gerfen, G. J.; Griffin, R. G.; Force, D. A.; Britt, R. D. *J. Phys. Chem. B* **1997**, *101*, 6634−6641.
(38) Deisenhofer, J.; Epp, O.; Miki, K.; Huber, R.; Michel, H. *Nature* **1985**, *318*, 618−624.

(39) Koepke, J.; Hu, X.; Munke, C.; Schulten, K.; Michel, H. *Structure* **1996**, *4*, 581−597.
(40) Kratz, W.; Myer, J. *J. Botany* **1955**, *42*, 282−287.
(41) Daboll, H. F.; Crespi, H. J.; Katz, J. J. *Biotech. Bioeng.* **1962**, *4*, 218−297.
(42) Tamura, N.; Cheniae, G. *Biochim. Biophys. Acta* **1987**, *890*, 179−194.
(43) Sanakis, Y.; Petrouleas, V.; Diner, B. A. *Biochemistry* **1994**, *33*, 9922−9928.
(44) Utschig, L. M.; Greenfield, S. R.; Tang, J.; Laible, P. D.; Thurnauer, M. C. *Biochemistry* **1997**, *36*, 8548−8558.
(45) Straley, S. C.; Parson, W. W.; Mauzerall, D. C.; Clayton, R. K. *Biochim. Biophys. Acta* **1973**, *305*, 597−609.
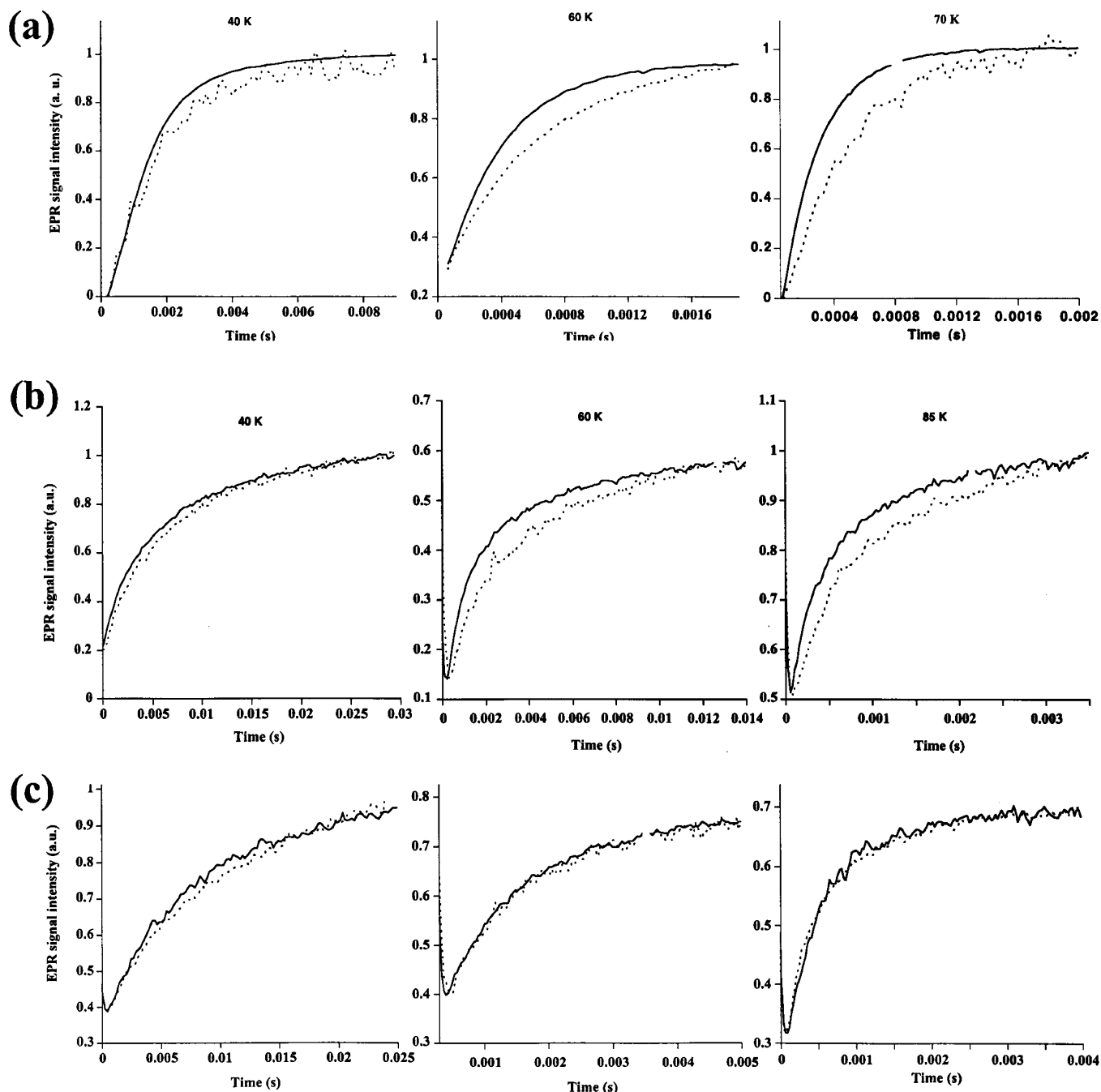
Figure 2. High-frequency (130 GHz) saturation-recovery transients of (a) Tyr$_D^\bullet$ in cyanide-treated (dotted line) and untreated (solid line) PS II at 40 K (left), 60 K (center) and 70 K (right), (b) Car$^+$ in cyanide-treated (dotted line) and untreated (solid line) PS II at 40 K (left), 60 K (center) and 85 K (right) and (c) Chl$^+$ in cyanide-treated (dotted line) and untreated (solid line) PS II at 40 K (left), 60 K (center) and 85 K (right).

ments were performed on PS II samples illuminated at 85 K (Figure 2).

Rb. sphaeroides R-26 reaction center samples for high-frequency D-band EPR measurements were placed in 0.55 mm I. D. quartz capillary tubes. The concentration of the reaction center protein was ~0.05 mM in buffer containing 10 mM TRIS at pH 8.0 with 0.045% LDAO. For generation of the P$_{865}^+$ radical species, the samples were pre-illuminated at room temperature in the EPR cavity and were rapidly frozen under illumination.

Pulsed D-Band High-Frequency EPR Spectroscopy. Pulsed high-frequency EPR spectra were obtained on a home-built D-band (130 GHz/4.5 T) continuous-wave (*cw*)/pulsed instru-

ment previously described elsewhere.[4,46] The maximum output power of the resonator in the pulsed mode is 125 mW (34 ns π/2 pulses) and 3.4 mW in the *cw* mode. The TE$_{011}$ cavity has several slits to allow for optical excitation and field modulation. An optical parametric oscillator (Opotek) pumped by a Nd:YAG laser (Quantel) was used for optical excitation. The output of the laser was coupled to a fiber optic in order to deliver light to the cavity (~1 mJ per pulse). The optical excitation wavelength was set to 550 nm. The EPR cavity temperature was regulated

(46) Poluektov, O. G.; Utschig, L. M.; Schlesselman, S. L.; Lakshmi, K. V.; Brudvig, G. W.; Kothe, G.; Thurnauer, M. C. *J. Phys. Chem. B* **2002**, *106*, 8911−8916.

by a temperature controller (Oxford ITC 503) coupled to a continuous helium-flow cryostat (Oxford CF 1200).

Direct measurement of long-range inter-spin distances between pairs of fast- and slow-relaxing spins in PS II and the bacterial reaction center were carried out using a three-pulse echo-detected saturation-recovery ((saturation-pulse)-(π/2)-τ-(π)-τ-echo) sequence. The echo pulses were in the range of 140 ns and 160 ns, respectively, with an inter-pulse echo delay (τ) of 400 ns. Measurement of spin−lattice relaxation rates in a rigid matrix is complicated as the inhomogeneous line width of the slow-relaxing spin is always greater than the B_1 field of the microwave pulses used in a saturation-recovery experiment. Under these conditions, saturation recovery is a hole-burning experiment and spectral-diffusion can interfere with the measured T_1 evolution. Long saturation pulses[47−49] or a string of picket-fence pulses[50−52] have previously been used to suppress contributions from cross-relaxation and spectral-diffusion processes in saturation-recovery EPR.[33] The dependence of the spin−lattice relaxation rate of Tyr$_D$• on the duration of the saturation-recovery pulse of the echo-detected saturation-recovery sequence was investigated in this study. The spin−lattice relaxation rate of Tyr$_D$• was studied as a function of saturation pulse length ranging from 140 ns to 10 ms (data not shown). It was found that the spin−lattice relaxation rate reaches a constant minimum with 5 ms or longer saturation pulse lengths. A 10 ms saturation pulse length was used to eliminate interference from spin-diffusion effects in recording of spin−lattice relaxation transients of Tyr$_D$•, Car$^+$, Chl$^+$, and P$_{865}^+$ in PS II and in purple bacterial reaction centers, respectively.

The magnetic-field position for the saturation-recovery measurements was set to 46 418 and 46 454 G for Car$^+$ and Chl$^+$ radicals in PS II, respectively, as indicated in Figure 1. The magnetic-field position for saturation-recovery measurements was set at the g_X and g_Y turning points for Tyr$_D$• in PS II (as indicated in Figure 4a) and the magnetic-field position was set at different points on the P$_{865}^+$ powder spectrum (as indicated in Figure 3a) for saturation-recovery measurements of P$_{865}^+$ in the purple bacterial reaction center samples. A nonlinear regression program written by Dr. Donald Hirsh employing the Marquardt algorithm[53] was used to fit saturation-recovery transients to a dipolar model[32] to obtain intrinsic and dipolar-enhanced spin−lattice relaxation rates for the interacting slow-relaxing spins.

Results and Discussion

Figure 1a−b show experimental high-frequency (130 GHz) *cw* light-minus-dark EPR difference spectra of Car$^+$ and Chl$^+$ radicals in PS II illuminated at 85 and 190 K, respectively. Shown in Figure 1c are simulated EPR spectra using the **g**-tensors of Car$^+$ and Chl$^+$ radicals in PS II reported previously.[4] As can be seen upon comparison of the composite EPR
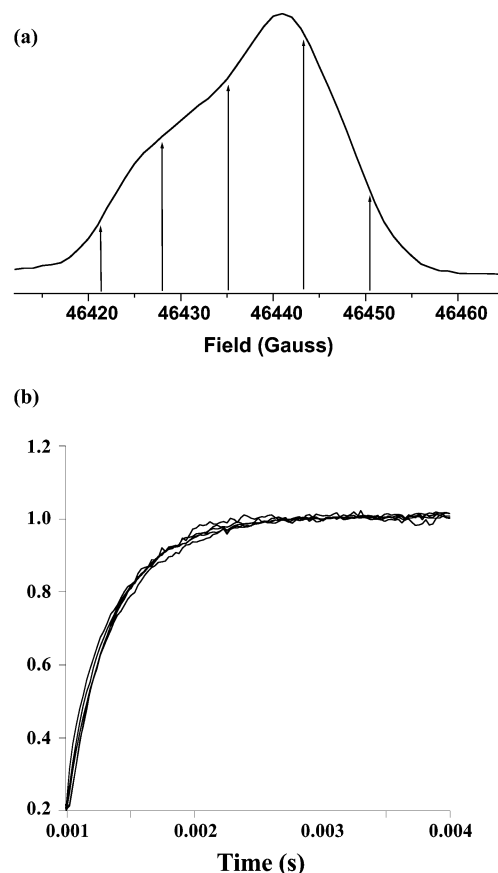
(47) Beck, W. F.; Innes, J. B.; Lynch, J. B.; Brudvig, G. W. *J. Magn. Reson.* **1991**, *91*, 12−29.
(48) Dalton, L. R.; Kwiram, A. L.; Cowen, J. A. *Chem. Phys. Lett.* **1972a**, *14*, 77−81.
(49) Dalton, L. R.; Kwiram, A. L.; Cowen, J. A. *Chem. Phys. Lett.* **1972b**, *17*, 495−499.
(50) Smigel, M. D.; Dalton, L. A.; Dalton, L. R. *Chem. Phys.* **1974**, *6*, 183−192.
(51) Percival, P. W.; Hyde, J. S. *Rev. Sci. Instrum.* **1975**, *46*, 1522−1529.
(52) Hung, S.-C.; Grant, C. V.; Peloquin, J. M.; Waldeck, A. R.; Britt, R. D.; Chan, S. I. *J. Phys. Chem. A* **2000**, *104*, 4402−4412.
(53) Press: W. H.; Flannery, B. P.; Teukolsky, S. A.; Vetterling, W. T. *Numerical Recipes in Pascal*; Cambridge University Press: Cambridge, 1989.
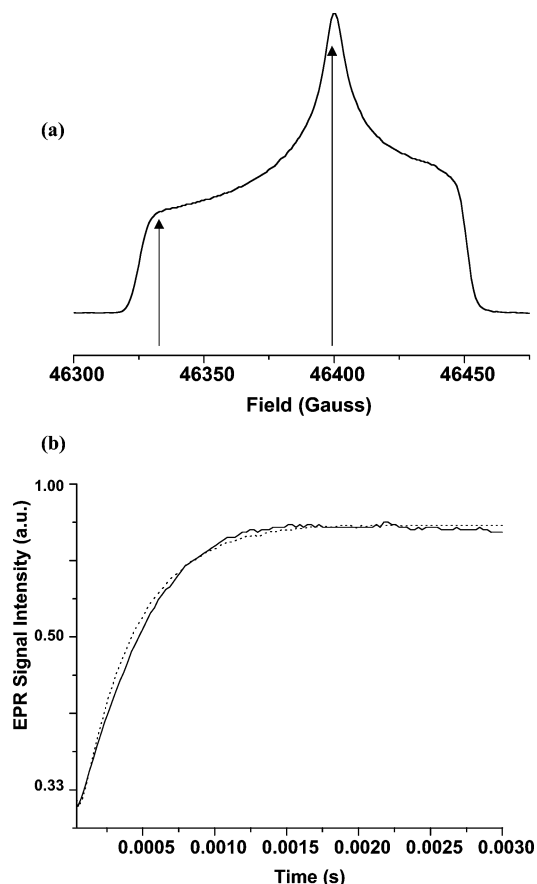
Figure 3. (a) Experimental high-frequency (130 GHz) pulsed-echo-detected EPR powder spectrum of P$_{865}^+$ radicals in the bacterial reaction center from *Rb. sphaeroides*. The arrows highlight the magnetic-field positions used for saturation-recovery measurements shown in (b).

line shapes of the experimental difference spectra (in Figure 1a−b) and the simulated contributions from the Car$^+$ and Chl$^+$ radicals (in Figure 1c), the low- and high-field regions of the spectra indicated by the dashed lines are from Car$^+$ and Chl$^+$ radicals, respectively. In the present study, the magnetic-field positions shown by the dashed lines assigned to Car$^+$ (46 418 G) and Chl$^+$ (46 454 G) radicals in Figure 1 are used for measurement of the spin−lattice relaxation rates of the cation radicals in the absence and in the presence of high-spin (*S* = 2) non-heme Fe(II) in PS II.

Measurement of Dipolar-Enhanced Spin−Lattice Relaxation Rates. It has previously been demonstrated that spin−spin interactions between a pair of slow- and fast-relaxing spins results in spin−lattice relaxation enhancement of the slow-relaxing spin.[32] The observed spin−lattice relaxation rate of the slow-relaxing spin ($k_{1,obs}$) (e.g., Tyr$_D$•, Car$^+$ and Chl$^+$) in the presence of the fast-relaxing spin (e.g., (*S* = 2) Fe(II)) is a combination of intrinsic ($k_{1,int}$) and dipolar- plus exchange-enhanced ($k_{1,ss}$) spin−lattice relaxation rate (eq 1)

$$k_{1,obs} = k_{1,int} + k_{1,ss} \qquad (1)$$

In the case of long-range spin−spin interactions (*r* > 20 Å) considered in this study, the exchange contribution to the spin−lattice relaxation rate is negligible. The dipolar spin−lattice relaxation rate ($k_{1,dipolar}$) is a function of the orientation of inter-spin vector in the applied magnetic field and all orientations

Figure 4. (a) Experimental high-frequency (130 GHz) pulsed-echo-detected EPR powder spectrum of dark stable $Y_D^•$ radicals in PS II. The arrows highlight magnetic-field positions used for the saturation-recovery measurements as shown in (b): g_X (solid line) and g_Y (dotted line), using the convention $g_X > g_Y > g_Z$.

are possible in a powder EPR sample. This results in multiexponential character of dipolar-enhanced spin−lattice relaxation transient of the slow-relaxing spin. $k_{1,dipolar}$ is also a function of the inter-spin distance (eq 2)

$$k_{1,dipolar} \, \alpha \, 1/r^6 \qquad (2)$$

Knowledge of relaxation times of the fast-relaxing spin (T_{1f} and T_{2f}) and Larmor frequency of the two spins (ω_s and ω_f) can enable direct measurement of the distance between the slow- and fast-relaxing spins.[32] We use high-frequency saturation-recovery EPR to investigate the interaction of slow-relaxing Car^+ and Chl^+ cofactor radicals with fast-relaxing non-heme Fe(II) in PS II. In addition to low-spin slow-relaxing radicals such as $Tyr_D^•$, Car^+, and Chl^+, PS II contains intrinsic high-spin fast-relaxing paramagnetic centers, namely, the tetranuclear manganese cluster (in the S_1 state) and the non-heme Fe (II) center. It has previously been shown that manganese depletion can be used to eliminate magnetic interaction with the tetra-nuclear manganese cluster of PS II.[54] It has also been shown that cyanide treatment can be used for conversion of high-spin ($S = 2$) form of Fe(II) to low-spin ($S = 0$) form of Fe(II).[43] In this study, manganese depletion of PS II is used to isolate solely the magnetic interaction of photoinduced $Tyr_D^•$, Car^+ and Chl^+

(54) Beck, W. F.; Innes, J. B.; Brudvig, G. W. In *Current Research in Photosynthesis*, Baltscheffsky, M., Ed.; Kluwer Academic Publishers: Dordrecht, The Netherlands, 1990; Vol. 1, pp 817−820.

radical with the non-heme Fe(II) and cyanide treatment in conjunction with manganese depletion is used to compare the intrinsic and dipolar-enhanced spin lattice relaxation rate of $Tyr_D^•$, Car^+, and Chl^+ radical in the presence of both low-spin ($S = 0$) and high-spin ($S = 2$) non-heme Fe(II), respectively.

As can be seen in Figure 2a, comparison of the spin−lattice relaxation transient of $Tyr_D^•$ in the absence and in the presence of the high-spin ($S = 2$) Fe(II) at different temperatures indicates enhanced spin−lattice relaxation of $Tyr_D^•$ due to dipolar interaction with the high-spin ($S = 2$) form of Fe(II). The saturation-recovery transients of $Tyr_D^•$ in the presence of high-spin ($S = 2$) Fe(II) exhibit multiexponential kinetics at different temperatures. Similarly in Figure 2b, comparison of spin−lattice relaxation transients of Car^+ in the presence of the high-spin ($S = 2$) Fe(II) and low-spin ($S = 0$) Fe(II) indicate enhanced spin−lattice relaxation of Car^+ radicals at 60 and 85 K due to dipolar interaction with high-spin ($S = 2$) Fe(II). Comparison of the saturation-recovery transient of Car^+ in the presence of high-spin ($S = 2$) Fe(II) (Figure 2b) with the saturation-recovery transient of $Tyr_D^•$ in the presence of high-spin ($S = 2$) Fe(II) (Figure 2a) indicates that the Car^+−Fe(II) dipolar interaction is weaker than the $Tyr_D^•$−Fe(II) dipolar interaction in PS II. This suggests that the Car^+−Fe(II) distance is greater than the known $Tyr_D^•$−Fe(II) distance in PS II of 37 Å.[23,35]

In contrast to Figure 2a−b, comparison of the saturation-recovery transient of Chl^+ in the presence of high-spin ($S = 2$) Fe(II) with the saturation-recovery transient in the presence of low-spin ($S = 0$) Fe(II) at different temperatures (Figure 2c) indicates that the Chl^+ radical displays negligible spin−lattice relaxation enhancement upon interaction with high-spin ($S = 2$) Fe(II). Qualitatively, the weak dipolar-enhancement of the spin−lattice relaxation of the Chl^+ radical in the presence of high-spin ($S = 2$) Fe(II) suggests that the Chl^+ radicals generated in the secondary electron-transfer pathway of PS II are ≥40 Å from the high-spin ($S = 2$) Fe(II) in PS II.

Effect of g-Anisotropy of Slow-Relaxing Spin on Spin−Lattice Relaxation Measurements. The dipolar model[32] that accounts for multiexponential saturation-recovery spin−lattice relaxation transients observed for a pair of interacting spins can be applied to obtain $Tyr_D^•$−Fe(II) and Car^+−Fe(II) inter-spin distances in PS II. However, a potential complication in the analysis of high-frequency saturation-recovery EPR transients is the presence of **g**- and **A**-anisotropy in the slow- and fast-relaxing spins. The dipolar model previously described by Hirsh et al. considers isotropic spins in defining the dipolar interaction between a pair of interacting spins.[32] Most slow-relaxing spins studied to date by X-band (9 GHz) saturation-recovery EPR have been organic radicals with small **g**- and **A**-anisotropy. At 130 GHz, however, the microwave pulses are narrow compared to the width of the EPR signal. It is possible that the presence of **g**-anisotropy in the slow-relaxing spin observed at high EPR frequency could restrict sampling of possible orientations to only a small subset of angles. Angle selection at 140 GHz has been previously used to demonstrate the presence of isotropic exchange-coupling contribution to the interaction of $Tyr^•$ and the diiron (Fe$_2$) cluster in ribonucleotide reductase from *yeast* and *E. coli*.[55] However, the influence of **g**-anisotropy and angle selection of a slow-relaxing spin on the observed dipolar-coupling contribution to spin−lattice relaxation in a saturation-

recovery experiment has previously not been characterized at high EPR frequency.

We investigate the P_{865}^+–Fe(II) and $Tyr_D^\bullet$–Fe(II) interactions in the bacterial reaction center from *Rb. sphaeroides* and PS II, respectively, to estimate the effect of the **g**-anisotropy of the slow-relaxing spin on the dipolar-enhanced spin–lattice relaxation transients at D-band EPR frequency. As can be observed in the echo-detected EPR powder pattern in Figure 3a, the P_{865}^+ radical in the bacterial reaction center displays **g**-anisotropy at 130 GHz EPR frequency.[46] Figure 3b displays the effect of **g**-anisotropy on the observed dipolar-enhanced saturation-recovery transients of P_{865}^+ in the presence of high-spin ($S = 2$) Fe(II). The observed spin–lattice relaxation transients of P_{865}^+ in the presence of high-spin ($S = 2$) Fe(II) collected at different magnetic-field positions (shown by arrows in Figure 3a) in the P_{865}^+ powder spectrum indicate only a small influence of **g**-anisotropy on the dipolar-enhanced spin–lattice relaxation rate of P_{865}^+.

Similarly, shown in Figure 4a is an echo-detected EPR powder pattern of $Tyr_D^\bullet$ in PS II. The spectral width of the powder pattern indicates significant **g**-anisotropy in the $Tyr_D^\bullet$ signal at 130 GHz EPR frequency.[56] Comparison of spin–lattice relaxation transients of $Tyr_D^\bullet$ interacting with high-spin ($S = 2$) Fe(II) in PS II with the magnetic-field position set at the g_X and g_Y turning points of $Tyr_D^\bullet$ powder spectrum (shown by arrows in Figure 4a) indicates a small influence of **g**-anisotropy on the dipolar-enhanced relaxation rate of $Tyr_D^\bullet$ radicals. On the basis of the small orientation dependence observed in Figures 3b and 4b, it is concluded that angle selection has minimal effect on measured spin–lattice relaxation rate of P_{865}^+ and $Tyr_D^\bullet$ interacting with high-spin Fe(II). The diminished effect of **g**-anisotropy of the slow-relaxing spin on the dipolar-enhanced spin–lattice relaxation rate of both $Tyr_D^\bullet$ and P_{865}^+ in the presence of high-spin ($S = 2$) Fe(II) in PS II and the bacterial reaction center, respectively, is most likely because the dominant effect is the anisotropy of the high-spin ($S = 2$) non-heme Fe-(II) in both proteins. This suggests that approximate distance estimates can be obtained using the isotropic dipolar model previously developed by Hirsh et al.[32]

Temperature Dependence of $k_{1,int}$ and $k_{1,dipolar}$ at D-Band EPR Frequency. To probe the differences in spin–lattice relaxation behavior at low and high EPR frequency, we compare the temperature dependence of the intrinsic and dipolar-enhanced spin–lattice relaxation rates of $Tyr_D^\bullet$ and $Tyr_D^\bullet$-Fe(II) at D-band EPR frequency to previously published spin–lattice relaxation rates of $Tyr_D^\bullet$ and $Tyr_D^\bullet$-Fe(II) at X-band EPR frequency.[32] The $k_{1,int}$ and $k_{1,dipolar}$ spin–lattice relaxation rates of $Tyr_D^\bullet$ are determined by fitting $Tyr_D^\bullet$ saturation-recovery transients to the isotropic dipolar model proposed by Hirsh et al.[32] The temperature dependence of the intrinsic ($k_{1,int}$) and dipolar ($k_{1,dipolar}$) spin–lattice relaxation rates are probed over a temperature range of 30 K to 95 K at D-band EPR frequency and these data are compared with the relaxation rates in this temperature range previously published by Hirsh et al.[32] The temperature dependence of $k_{1,int}$ at both D-band and X-band EPR frequency displays similar $\sim T^{2.3}$ temperature dependence (Figure 5a). However, it appears that the magnitude of $k_{1,int}$ at D-band EPR

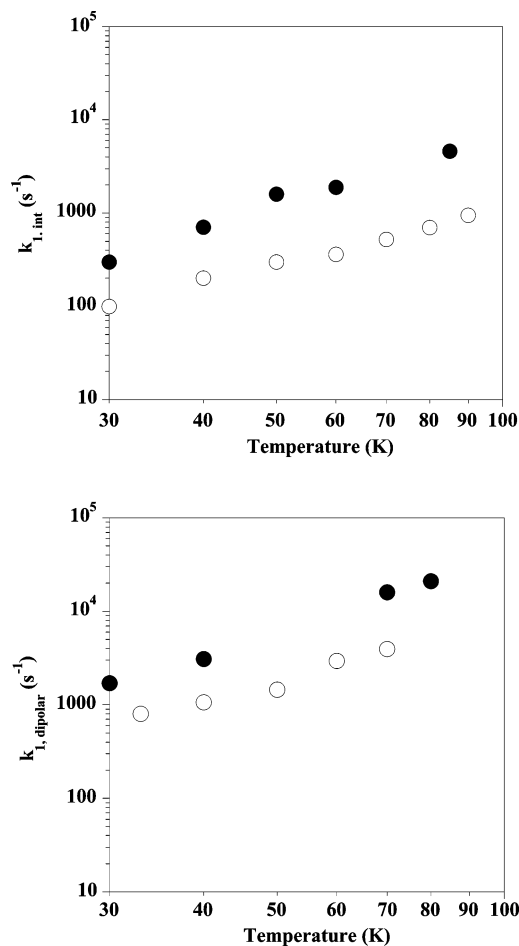**Figure 5.** Temperature dependence of (a) the intrinsic and (b) dipolar-enhanced spin–lattice relaxation rates of $Tyr_D^\bullet$ radicals in cyanide-treated, Mn-depleted, and Mn-depleted PS II, respectively, at D-band EPR frequency (filled circles). Also shown are the intrinsic and dipolar-enhanced spin–lattice relaxation rates of $Tyr_D^\bullet$ radicals in cyanide-treated, Mn-depleted and Mn-depleted PS II, respectively, at X-band EPR frequency (open circles). X-band saturation-recovery EPR data from Hirsh et al.[32]

frequency is a factor of 2.7 higher than $k_{1,int}$ at X-band EPR frequency.[32] The $k_{1,dipolar}$ relaxation rates exhibit similar changes in magnitude and temperature dependence at D-band and X-band EPR frequency[32] (Figure 5b). The difference in the slope of the temperature dependence of $k_{1,int}$ and $k_{1,dipolar}$ is further indication that the enhanced spin–lattice relaxation rate of $Tyr_D^\bullet$ is from the dipolar coupling between $Tyr_D^\bullet$ and the high-spin ($S = 2$) Fe(II) in PS II. The temperature dependence of $k_{1,dipolar}$ relaxation rate at D-band EPR frequency shown in Figure 5b indicates that the B-term is the correct limit for evaluation of $k_{1,dipolar}$.[32]

Effect of $S > 1/2$ Fast-Relaxing Spin on Dipolar Spin–Lattice Relaxation Measurements. It has been demonstrated by Eaton and Eaton[57] that the analysis of saturation-recovery transients can be different in the case of a fast-relaxing spin with $S > 1/2$ interacting with a slow-relaxing ($S = 1/2$) spin. For a fast-relaxing spin with $S > 1/2$, there is more than one Δm_S transition and each transition could have a different potential for inducing transitions in the slow-relaxing spin. Each

(55) Bar, G.; Bennati, M.; Nguyen, H.-H. T.; Ge, J.; Stubbe, J.-A.; Griffin, R. G. *J. Am. Chem. Soc.* **2001**, *123*, 3569–3576.
(56) Un, S.; Tang, X.-S.; Diner, B. A. *Biochemistry* **1996**, *35*, 679–684.

(57) Eaton, S. S.; Eaton, G. R. In *Distance Measurements in Biological Systems by EPR*; Berliner, L. J., Eaton, S. S. and Eaton, G. R., Ed.; Kluwer Academic/ Plenum Publishers: New York, 2000; Vol. 19 of Biological Magnetic Resonance, pp 29–154.

transition could also have different spin–lattice and spin–spin relaxation rates. The magnetic properties and relaxation rates of the high-spin ($S = 2$) Fe(II) in PS II have not been directly determined but it has been suggested that the magnetic properties of Fe(II) are similar in PS II and the reaction center from *Rb. sphaeroides*.[32] A useful approach demonstrated by Hirsh and Brudvig in the X-band saturation recovery analysis of reaction centers from *Rb. sphaeroides* and PS II has been to use the data for the P_{865}^+–Fe(II) interaction in the structurally characterized bacterial reaction center to calibrate the $Tyr_D^\bullet$–Fe(II) interaction in manganese-depleted PS II.[32] This approach avoids complications encountered in the direct determination of magnetic parameters of the high-spin ($S = 2$) Fe(II) and has been shown to result in accurate measurement of inter-spin distances in PS II. For example, by using the P_{865}^+–Fe(II) distance in bacterial reaction centers as a calibration, the $Tyr_D^\bullet$–Fe(II) and $Tyr_Z^\bullet$–Fe(II) distances in PS II at X-band EPR frequency were both estimated to be 37 ± 5 Å.[35] These distances are in excellent agreement with the X-ray crystal structure of PS II (Tyr_D–Fe(II) and Tyr_Z–Fe(II) center-to-center distances of 37.5 Å).[23]

Relative Location of Car$^+$ Radicals in PS II. The present study indicates that the Car$^+$–Fe(II) and Chl$^+$–Fe(II) distances are greater than the known $Tyr_D^\bullet$–Fe(II) distance of ~37 Å in PS II. Upon calibration with the known $Tyr_D^\bullet$–Fe(II) dipolar distance and the dipolar-enhanced spin–lattice relaxation rate of $Tyr_D^\bullet$ determined from the temperature-dependent plot in Figure 5b, we estimate that the Car$^+$–Fe(II) and Chl$^+$–Fe(II) distances in PS II are 38 ± 1 Å and ≥40 Å, respectively. The shorter distance of the Car$^+$ to the non-heme Fe(II) than Chl$^+$ is consistent with the Car being the earlier electron donor to P_{680}^+ than Chl.

The dipolar distances are weighted as $1/r^6$ and interpretation of these distances must take into account the spin distributions within the Car$^+$ and Chl$^+$ radicals. Hyperfine couplings determined from ENDOR studies and calculated spin densities of the individual carbon atoms of model Car$^+$ radicals have indicated that the unpaired electron spin is distributed over the entire length of the polyene chain of model carotenoid cation radicals.[21] This observation is also supported by resonance Raman spectroscopic studies conducted on Car$^+$ radicals in solution that have indicated that the charge is evenly distributed over the polyene chain.[22] Similarly, hyperfine couplings obtained from pulsed ENDOR studies on Chl a^+ in vitro and Chl$^+$ radicals in PS II indicate that the spin density is distributed over the tetrapyrrole ring of the chlorophyll molecule.[7] To evaluate the effect of these spin distributions on the calculated distances, we have performed distributed dipole–dipole calculations using the Chl$^+$ and Car$^+$ spin densities previously determined[7,21] with different distances and orientations of each cofactor relative to the non-heme Fe(II). These calculations show that the large value of the dipolar distance we obtain for Chl$^+$–Fe(II) relative to the size of the Chl$^+$ molecule makes interpretation of the dipolar distance as the center-to-center Chl$^+$–Fe(II) distance a valid approximation in the present study. However, the spin of Car$^+$ is distributed over the conjugated carbon atoms of the polyene chain, which extends approximately 23 Å in an all-trans configuration. A series of tilt angles of a linear all-trans Car$^+$ relative to the center-to-center interspin vector was compared while maintaining a constant center-to-center Car$^+$–
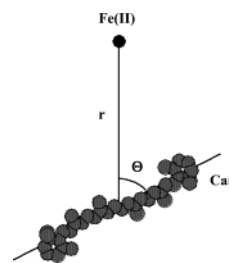

Figure 6. Relative orientation of a linear all-trans Car$^+$ relative to the center-to-center Car$^+$–Fe(II) interspin vector in PS II. The Car$^+$ tilt angle (Θ) was varied for the distributed dipole calculations, whereas maintaining a constant center-to-center Car$^+$–Fe(II) distance (r) of 38 Å.

Fe(II) distance of 38 Å (Figure 6). These calculations show that Car$^+$ with a tilt angle of 0° is equivalent to the point dipole approximation with a distance of 38 Å. Rotation of the Car$^+$ about the interspin vector places one end of the Car$^+$ progressively closer to the non-heme Fe(II). A rotation of ≤30° gave a dipolar coupling within error of the point dipole approximation, but a larger tilt resulted in a dipolar coupling that was greater than the experimentally observed coupling. On the other hand, at a 90° orientation with the center-to-center Car$^+$–Fe(II) distance of 38 Å, one end of the Car$^+$ extends beyond the surface of the D1/D2 subunits of PS II. We can conclude that either the Car$^+$ is oriented approximately within the membrane plane with a center-to-center Car$^+$–Fe(II) distance of 38 Å or that the Car$^+$ is tilted with a center-to-center Car$^+$–Fe(II) distance greater than 38 Å. With regard to the tilt angle of the Car$^+$, linear dichroism measurements have suggested that one of the two β-carotene molecules in the D1/D2 subunits is oriented approximately parallel to the membrane plane and the other is tilted at an angle of approximately 45°.[12,13]

It was previously thought that only Chl and Cyt b_{559} cofactors are involved in the secondary electron-transfer pathway of PS II. On the basis of this assumption, Koulougliotis et al. used progressive power-saturation and saturation-recovery EPR experiments at X-band EPR frequency to determine the location of Chl_Z^+ in PS II.[36] At X-band EPR frequency, Chl_Z^+ and Car$^+$ radicals display overlapping EPR signals that result in a single featureless resonance in the $g = 2$ region of the spectrum.[8,36] Saturation-recovery spin–lattice transients of Chl_Z^+ at X-band EPR frequency presented evidence for dipolar-enhanced spin–lattice relaxation of Chl_Z^+ in the presence of high-spin ($S = 2$) Fe(II) that is absent in the presence of low-spin ($S = 0$) Fe(II) in PS II. Using the P_{865}^+–Fe(II) dipolar interaction in the reaction center from *Rb. sphaeroides* as a calibration, the Chl_Z–Fe(II) distance in PS II at X-band EPR frequency was determined to be 39 ± 2.5 Å.[36] The center-to-center Chl_Z^+–Fe(II) and Chl_D^+–Fe(II) distances determined by Zouni et al. are 40.4 and 40.0 Å, respectively.[23] The Chl_Z^+ radicals in the X-band EPR study by Koulougliotis et al. were generated by illumination of PS II samples at 77 K with the Cyt b_{559} heme center in the preoxidized state.[36] More recently, it has been shown that illumination of PS II samples at 77 K with the Cyt b_{559} heme center preoxidized generates a mixture of Car$^+$ and Chl$^+$ radicals.[4,9] Thus, the Chl_Z–Fe(II) dipolar distance of 39 ± 2.5 Å determined in the previous X-band saturation-recovery EPR study was a weighted average of the Car$^+$–Fe(II) and Chl$^+$–Fe(II) distances in PS II. The high-frequency saturation-recovery EPR distance estimates of 38 ± 1 Å and ≥40 Å for the Car$^+$–Fe(II) and Chl$^+$–Fe(II) distances, respectively, are
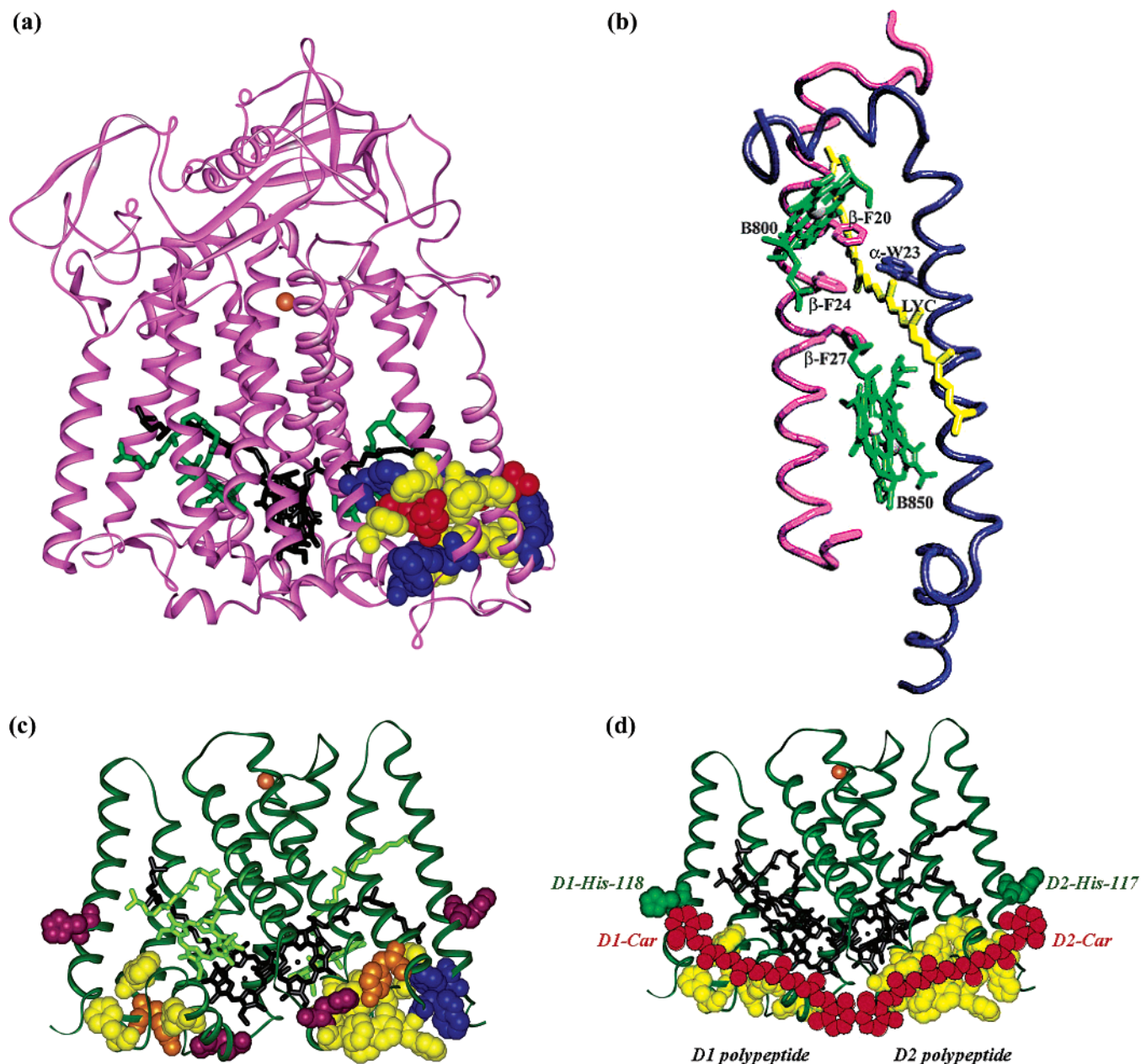
(a)

(b)

(c)

(d)

Figure 7. (a) Sphaeroidene-binding pocket of the bacterial reaction center from *Rps. viridis*[38] (pdb code: 1prc). The sphaeroidene is shown in red with neighboring tryptophan (blue) and phenylalanine (yellow) residues that form the binding pocket. Also shown are the bacteriochlorophyll (black), accessory bacteriochlorophyll (green) and non-heme Fe(II) (orange) centers in the reaction center. (b) The lycopene-binding pocket of the light-harvesting-II complex from *Rhodospirillum molischianum*[39] (Figure adapted from Wang and Hu, 2002).[58] The bacteriochlorophyll pigments (B$_{850}$ and B$_{800}$) flanking the lycopene molecule are shown in green. The tryptophan and phenylalanine residues in the lycopene-binding pocket are highlighted in blue and pink, respectively. (c) The location of the putative β-carotene binding pockets in photosystem II[59] (pdb code: 1dop) are shown by highlighting the position of neighboring aromatic amino acid residues that may line the binding pocket (tryptophan, tyrosine, phenylalanine and histidine residues are shown in blue, orange, yellow and magenta, respectively). Also shown are His-117 and His-118 residues that ligate the monomeric chlorophyll cofactors on the D2 and D1 polypeptides of PS II, respectively. The location of the special pair of primary-donor chlorophylls (black), accessory chlorophylls (green) and non-heme Fe(II) (orange) in PS II are shown in this figure. (d) The possible positions of the redox-active β-carotene cofactor in the putative binding sites that are shown in Figure 7(c). The amino acid residues lining the β-carotene binding pocket are shown in yellow and the β-carotene molecules are shown in red. The location of the primary donor chlorophyll molecules (black), the accessory chlorophylls (black), His-117 and His-118 residues that ligate the monomeric chlorophyll cofactors (green) and the non-heme Fe(II) (orange) in PS II are also shown in this figure.

consistent with the distance of 39 $\pm$ 2.5 Å, previously determined by X-band saturation-recovery EPR spectroscopy.[36]

Figure 7a depicts the X-ray crystallography structure of the reaction center from *Rps. viridis*[38] with the primary-donor chlorophyll pigments (P$_{865}$), accessory chlorophyll pigments and the non-heme Fe(II) shown in black, green and orange, respectively. We highlight the sphaeroidene molecule in red and the tryptophan and phenylalanine residues that line the sphaeroi-

dene-binding pocket in blue and yellow, respectively. The center-to-center distance between the sphaeroidene and the non-heme Fe(II) in the reaction center is $\sim$32 Å. Shown in Figure 7b is the X-ray crystallography structure of the carotenoid-binding pocket in the LH−II complex from *Rhodospirillum molischianum*.[39] The bacteriochlorophyll pigments (B$_{850}$ and B$_{800}$), tryptophan and phenylalanine residues are highlighted in green, blue, and pink, respectively. The carotenoid-binding

pocket of the purple bacterial reaction center[38] and the light-harvesting complex II (LH−II)[39] shown in Figure 7a and 7b, respectively, indicate that carotenoids in pigment−protein complexes are either surrounded by aromatic residues or by bacteriochlorophyll molecules (with extensive π-conjugation). These observations combined with intermolecular interaction energies calculated by ab initio methods suggest that $\pi-\pi$ stacking interactions are the molecular forces that bind carotenoids in photosynthetic pigment−protein complexes.[58]

On the basis of the distance estimates obtained in the present study and by analogy with the location and structure of the carotenoid-binding pocket of the bacterial reaction center from *Rps. viridis*[38] and the LH−II complex from *Rhodospirillum molischianum*,[39] we identify possible binding sites for the two β-carotene molecules in the D1/D2 core of PS II. Previous 2D-ESEEM results and numerical simulations of the Car^+ radical in PS II indicate that the Car^+ radical of PS II interacts with one protein ^{14}N nucleus ($e^2qQ/h = 3.09$ MHz) that is assigned to be the indole ^{14}N of a tryptophan residue.[16] This study had suggested that D2-Trp-112 and D2-Trp-168 (homologous to M-115 and M-171 in the purple bacterial reaction center, respectively) and D2-Trp-49 and D2-Trp-59 (homologous to M-66 and M-75 in the purple bacterial reaction center, respectively) could be potential candidates for these ^{14}N magnetic couplings observed in the 2D-ESEEM study. On the basis of the $\sim$38 Å Car^+-Fe(II) distance estimated by high-frequency saturation-recovery EPR measurements, we eliminate the possibility of D2-Trp-49, D2-Trp-59, and D2-Trp-112 residues forming the pocket for the redox-active Car^+ radical in PS II because these residues are only 16−24 Å from the non-heme Fe(II).[23] However, D2-Trp-168 is located at the correct distance from the non-heme Fe(II) to form the carotenoid binding site. A search for neighboring aromatic amino acid residues in the vicinity of D2-Trp-168 of PS II reveals a hydrophobic patch comprised of Tyr-161, His-190, Phe-174, Phe-170, Phe-169, Phe-189, Phe-185, and Phe-182 on the D2 polypeptide. These amino acid residues are highlighted in Figure 7c based on the theoretical model of PS II of Svensson et al.[59] As can be seen in Figure 7c, there is a similar but less extensive patch of hydrophobic residues at a symmetric location on the D1 polypeptide of PS II. Shown in Figure 7d are two possible locations and orientations of the redox-active β-carotene molecule in the putative β-carotene binding pockets of PS II that are shown in Figure 7c. Binding of two copies of β-carotene in the possible binding sites in the orientations indicated in Figure 7d could allow the ends of the carotenoid molecules to be positioned close to each other. This would be consistent with

observations from circular dichroism that the two Car molecules are excitonically coupled and may be placed in close proximity of each other in the PS II reaction center.[14]

It is thought that since the sphaeroidene is involved in a triplet-quenching energy-transfer mechanism in the bacterial reaction center, it is located in close proximity to the bacteriochlorophyll primary donor, P_{865} ($r_{center-to-center} \approx 19$ Å from the X-ray crystal structure). In contrast, the putative β-carotene-binding sites in PS II are at a greater distance from the primary-donor chlorophyll, P_{680} (Figure 7c). The greater separation between the carotenoid and P_{680} in PS II is consistent with the observation that the Car does not quench triplets in PS II.[60]

If the Car binds in the putative binding pocket in the D2 polypeptide as described in Figure 7c−d, this places the Car between P_{680}, Chl_D and Cyt b_{559}. This would aid long-range cyclic electron transfer to P_{680}^+ from Cyt b_{559} and Chl_D as the distance between these cofactors is >30 Å. The proximity of the Car to P_{680} is consistent with its role as an intermediate electron donor. In addition, the Car-binding pockets on the D1 and D2 polypeptide are proximal to each other and both the monomeric Chls (Chl_D and Chl_Z) that could enable participation of the β-carotene molecules as molecular wires in rapid hole-equilibration among the secondary electron donors on either side of the hetero-dimer of PS II (Scheme 1).

Abbreviations. Car: β-carotene; Chl: monomeric chlorophyll; cw: continuous wave; β-DM: β-dodecyl maltoside; Cyt b_{559}: cytochrome b_{559}; D1: D1 polypeptide; D2: D2 polypeptide; ENDOR: electron−nuclear double-resonance; EPR: electron paramagnetic resonance; ESEEM: electron spin−echo envelope modulation; Fe(II): non-heme Fe(II) center; FTIR: Fourier-transform infrared; His: histidine; LDAO: lauryldimethylamine *N*-oxide; LH−II: light-harvesting II complex from *Rhodospirillum molischianum*; MES: 2-[N-morpholino] ethane sulfonic acid; P_{680}: primary-donor chlorophyll of PS II; P_{865}: primary-donor bacteriochlorophyll of the *Rb. sphaeroides* reaction center; Phe: phenylalanine; PS II: photosystem II; RC: reaction center; TRIS: tris (hydroxymethyl) aminomethane; Trp: tryptophan; Tyr: tyrosine

JA0295671

(58) Wang, Y.; Hu, X. *J. Am. Chem. Soc.* **2002**, *124*, 8445−8451.
(59) Svensson, B.; Etchebest, C.; Tuffery, P.; van Kan, P.; Smith, J.; Styring, S. *Biochemistry* **1996**, *35*, 14 486−14 502.
(60) Barber, J.; Archer, M. D. *J. Photochem. Photobiol. A-Chem.* **2001**, *142*, 97−106.